A Study of Crab Giant Pulses using the LWA

Logan Cordonnier, Cameron Lamar, Cameron Zamora

May 7, 2021

Abstract

We present a small study of giant pulses from the Crab Pulsar. We analyzed data acquired using both operating stations of the Long Wavelength Array (LWA1 and LWA-SV) at 60 and 76 MHz. After the data were reduced and processed, it was visually examined to search for giant pulses. Upon analyzing 6 hours of data from each of the two tunings, we characterized 96 pulses, 42 of which were unique. For each pulse, we derived its characteristic broadening time, then averaged these values to get $\tau = 213 \pm 67$ ms at 60 MHz, and $\tau = 127 \pm 44$ ms at 76 MHz. These values were then contextualized through the lens of previous studies done by both the LWA and other low frequency observations, where they were found to be in good agreement.

1 Introduction

1.1 Background on Pulsars

A pulsar is a neutron star which is highly magnetized and rotating very quickly. They emit highly regular pulses of radio emission with short periods (Condon & Ransom, 2016). According to Condon & Ransom (2016), the periods of these pulses range from 1.4 ms to 8.5 s. However, in 2018, Tan et al. published their discovery of "PSR J0250+5854, a radio pulsar with a spin period of 23.5 s" via the LOFAR Tied-Array All-Sky Survey (LOTAAS).

The rapidly pulsing emission from pulsars originates from the magnetic poles of the star. The neutron star emits beams of coherent emission along the magnetic axis (see Figure 1) caused by electrons that are accelerated along the open (also curved) field lines (Condon & Ransom, 2016). The acceleration from curvature is responsible for the emission of curvature radiation by the electrons (Condon & Ransom, 2016) — an emission mechanism that has some similarities to synchrotron radiation. The pulsing behavior is not caused by the emission turning on and off, but instead is a result of the neutron star's rotation. As can be seen in Figure 1, the rotation axis and magnetic axis of a pulsar are misaligned. This misalignment causes the beams of emission coming from the magnetic poles to sweep around the rotation axis as the star spins. Condon & Ransom (2016) describe how we see pulses from this sweeping beam with the following analogy to lighthouses: "Like lighthouses, they continuously emit rotating beams of radiation and appear to flash each time the beam sweeps across the observer's line of sight." They also state that this is why the pulse periods are usually very stable for pulsars — because they are the same as the rotation periods.

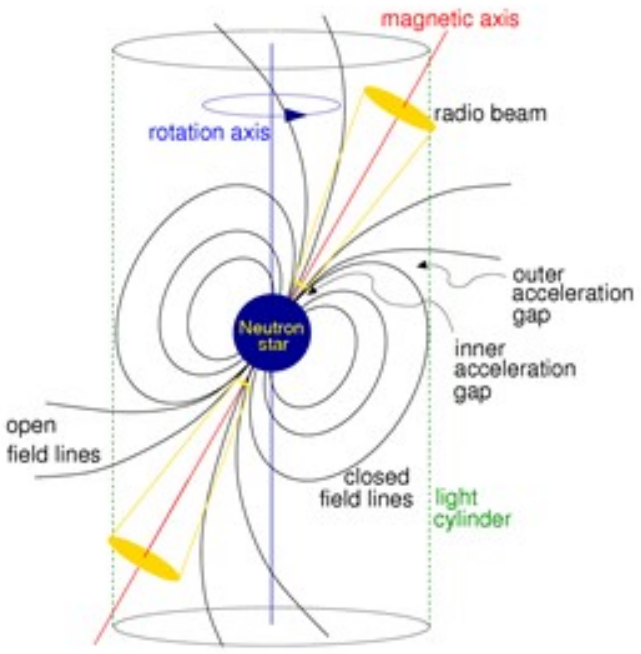

Figure 1: A model showing the structure of a pulsar. Credit: Lorimer & Kramer (2004)

1.2 Giant Pulses

According to Johnston & Romani (2004), a single pulse from a pulsar typically does not exceed the mean flux density of the source by more than a factor of 10 (excluding scintillation effects). However there are at least a handful of pulsars which exhibit pulses of greatly increased intensity. For example, the Crab Pulsar (which is the focus of this study) is known to exhibit pulses which "can exceed the average flux density by several orders of magnitude, becoming one of the brightest radio sources in the sky" (Eftekhari et al. 2016). These pulses of outstanding intensity are what we call "giant pulses" (a simple and fitting name). The Crab Pulsar was the only pulsar known to emit giant pulses for over 25 years, but many other giant pulse emitters are now known (Johnston & Romani, 2004).

1.3 Dispersion Measure

When making observations of the short-duration, broadband pulses from a pulsar, it is important to discuss the dispersion that the pulse undergoes on its journey to the detecting instrument. The interstellar medium (ISM) can be treated as a cold plasma with some index of refraction composed of the ISM electrons (see Condon & Ransom, 2016). Since this index of refraction is frequency dependent, the group velocity of an electromagnetic wave traveling through the ISM will also be frequency dependent. This causes dispersion of an incoming broadband pulse. The dispersion delay will be greater for photons of lower energy/higher frequency (Condon & Ransom, 2016). The overall effect of this dispersion can be seen in plots like that in Figure 2, from Eftekhari et al. (2016), where the pulse is detected slightly sooner for higher frequencies and is later detected at progressively lower frequencies.

A quantity often used to talk about how much dispersion happens in the medium between source and detector is the dispersion measure (DM), which "represents the integrated column density of electrons between the observer and the pulsar" (Condon & Ransom, 2016).

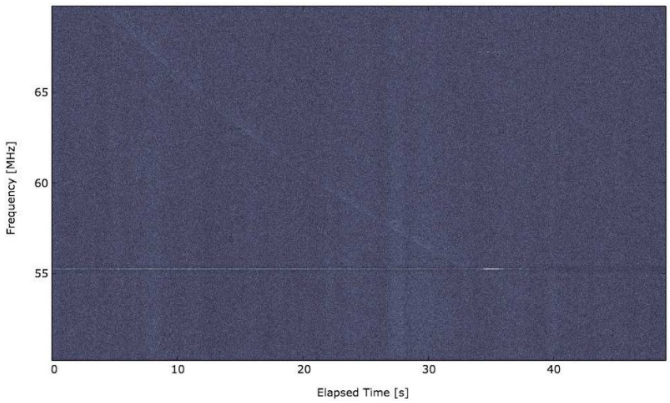

Figure 2: An example of a dispersed pulse. Credit: Eftekhari et al. (2016)

1.4 Modeling Pulse Shape for Low Frequencies

The varying density of electrons in the ISM causes a pulse to be broadened by scattering mechanisms throughout its journey to us (Eftekhari et al., 2016). Eftekhari et al. says that this mechanism is extremely frequency dependent (ν^{-4}), and thus broadening of an intrinsically narrow pulse is prevalent at low frequencies, where we have conducted our observations. A good model for pulse shape for frequencies less than 200 MHz (Eftekhari et al., 2016) is given by Eqn. (1)

$$g(t) = t^{\beta} exp(-t/\tau) u(t). \quad (1)$$

$u(t)$ is a step function which sets the pulse to be zero for all times before the pulse actually occurs. τ is a parameter called the characteristic broadening time which describes how long it takes a pulse to decay away. β is a parameter that describes how quickly the pulse begins to rise; that is, β describes how steep the rising edge of our pulse is.

2 Observations

2.1 Source

For our study we observed the Crab Pulsar (PSR B0531+21). The Crab is notorious for its giant pulses, and is a frequently studied pulsar. It is located at RA: 5h 34m 31.97s, Dec: +22° 0' 52" in the constellation Taurus.

2.2 Instrumentation

Our observations were taken using both operating stations of the Long Wavelength Array (LWA). Both stations (LWA1 and LWA-SV) consist of 256 dual-polarized dipole antennas spread out over a diameter of about 100 m, which operate as an interferometer. The LWA, as the name implies, is capable of operating at low frequencies (from 10-88 MHz). LWA1 is co-located with the Karl G. Jansky Very Large Array. LWA-SV is located at the Sevilleta National Wildlife Refuge.

2.3 Setup and Execution

Both LWA stations observed simultaneously, each with the same two tunings — 60 MHz and 76 MHz. Around each center frequency, we had bandwidths of 19.6 MHz, with only 16 MHz being usable due to bandpass filter effects (rolling over at each end of the bandwidth).

We observed the Crab Pulsar every other day for a total of 9 days (5 days of observations), beginning on February 28, 2021. For each of the 5 observing days, both stations observed using both tunings for 2 hours, centered about the transit of the Crab Pulsar for optimal viewing. This produced 40 hours of total data that could be analyzed.

Our group processed and analyzed only the data from the first day (Feb. 28) and the last day (Mar. 8) of observations for both stations and both tunings. However, there were considerable issues with the February 28 LWA-SV data, so it was not used.

3 Data Preparation

The first step in the data reduction process was to determine the value of DM to use for dedispersion. Due to the short pulse period of the crab pulsar (33.5 ms) and the low observational frequencies used, the normal pulses end up being temporally smeared (see Bansal et al. 2019) and are therefore indistinguishable. This means that traditional folding techniques, such as those applied in `prepfold`, are unable to determine a DM based on the normal periodic pulses. Though there is documented variability in the DM of the crab pulsar (Lyne et al., 1993), it was deemed to be relatively insignificant in light of other, more glaring uncertainties (which will be explored later). Eftekhari et al. (2016) reported a DM with an upper limit as high as 57.10 pc cm^{-3}, which

differs from the canonical value of 56.79 pc cm^{-3} by only about 0.5%. For this reason, the canonical DM value was used for dedispersion purposes.

The process used to transform the data into a usable form went as follows, with thanks to Pratik Kumar for suggesting the technique: the raw data (in DRX format) was first coherently dedispersed at the canonical DM value and was converted to the `PSRFITS` (.fits) format which is compatible with the utilities provide by the `PRESTO` software suite. Both of these tasks were accomplished via the `writePsrfits2D.py` routine found in the LWA Software Library (LSL). From here, the data were examined for radio frequency interference (RFI) which was subsequently masked out from future analyses. The `rfifind` utility from `PRESTO` was used to accomplish this - the data were binned into two second integration intervals and strong, transient signals were clipped. Incoherent dedispersion was then applied to the data using `PRESTO`'s `prepsubband`. Instead of shifting the arrival time for each individual frequency channel, this utility partially shifts subbands (or groups of channels) at the same time, which should save computation time; we used 256 subbands for this step. The output of `prepsubband` is a .dat file, which can then be visually examined using `exploredat`. This utility plots the data as a time-series and allows for interactive manipulation, such as zooming in/out and skipping through time. By default, the data is plotted along with the mean (averaged over about 9 data intervals) and the one sigma values. This plot was then skimmed through manually, and visually distinguishable giant pulses were recorded.

4 Analysis

The typical next step would be to perform regression analysis on the individual giant pulses using Eqn. (1) as the model equation. However, we ran into issues when attempting to access and manipulate the data stored in the .dat file, which meant that this regression technique was not feasible. Instead, Eqn. (1) was examined analytically for alternative methods of determining the characteristic pulse broadening time (τ). Finding τ values will allow for the results of this work to be compared to the large body of previous studies concerning Crab giant pulses, and therefore this is the primary goal of this section. To that end, the derivative of Eqn. (1) with respect to t was taken and set equal to zero in order to find the t value corresponding to the maximum of the function, as seen in Eqn. (2).

$$g'(t) = \frac{t^{\beta-1} exp(-t/\tau)(\beta\tau - t)}{\tau} = 0 \qquad (2)$$

Solving this for t gives $t = \beta\tau$. Plugging this back into the original expression (Eqn. (1)) gives the maximum value of the function, shown in Eqn. (3)

$$g_{max} = t_{max}^{\beta} exp(-t_{max}/\tau) = t_{max}^{\beta} e^{-\beta} \qquad (3)$$

This equation now only depends on one free parameter, β, which can be solved for. From here, τ can be worked out such that $\tau = t/\beta$. This then produces Eqn. (4):

$$\tau = \frac{t_{max} ln(g_{max})}{ln(t_{max}) - 1} \qquad (4)$$

Eqn. (4) is particularly useful since it relates τ to values which can be visually determined from the plot of the pulse; t_{max} is the amount of time it takes to get from the initial rise of the pulse to its maximum value, and g_{max} is the height of the pulse above the noise baseline leading up to the pulse. Though this technique eliminates the need to do a formal regression analysis, it introduces a new issue: determining these values involves a large degree of subjectivity. To help mitigate the amount of uncertainty in the measurement of t_{max} and g_{max}, a pixel ruler was used to accurately determine their values. This ruler displays the number of pixels between two points, and can be calibrated against the reference values given on the axes. However, despite being able to find the distances accurately, there is still the matter of determining which points to use in making these measurements. Therefore, the values of t_{max} and

g_{max} were recorded, as well as the estimated uncertainty which arises from manually choosing the location of these points. These uncertainties were propagated through Eqn. (4) in the usual way via the general formula for error propagation (see Taylor 1997 for details). The nature of the uncertainties is assumed to be random; in other words, we do not believe that there is any sort of systematic error present in our determinations of t_{max} and g_{max}. These errors represent a substantial error when viewed in the scope of a single pulse; however, when averaged over many pulses, it is expected that they will tend to cancel out and become relatively insignificant in comparison to the spread (standard deviation) of the pulses' τ values.

5 Results

The procedure outlined above was applied to both tunings (60 MHz and 76 MHz) of both stations (LWA1 and LWA-SV) on the first day of observation (February 28, 2021) and on the last day of observation (March 8, 2021). The three days of observation in between were not analysed in this present study due to time constraints. It should be noted that the data from LWA-SV was corrupted beyond repair for the first day of observations - however, it was operating normally for the observations made on the last day. This left six hours of observations for each frequency tuning to be analysed. Figure 3 shows a comparison of the same pulse for both tunings and both stations, to give a general idea of how these factors affect the nature of the pulse. As evidenced by the plots, the 60 MHz pulses are characterized by gentler turn over regions and shallower rising edges compared to the 76 MHz pulses. There is not much to distinguish between the two stations, as the pulse profiles match fairly well.

By visual inspection, a total of 96 giant pulses were identified and characterized in the aggregate 12 hours of observation (across both frequencies). Many of these represent the same physical pulse; accounting for this reduces this to 42 unique pulses. Figure 4 presents the average characteristic broadening time of these observations, broken down by station and day (where appropriate). It also provides the standard deviation of the τ measurements.

	60 Mhz		76 Mhz	
	τ (ms)	±σ (ms)	τ (ms)	±σ (ms)
LWA1, first day	235	65	142	28
LWA1, last day	205	54	129	44
LWA1, total	215	59	134	39
LWA-SV	211	77	116	49
Total (both stations)	213	67	127	44

Figure 4: Summary of broadening times

For a detailed breakdown of τ for each pulse, see Tables 1 and 2 (in Appendix).

6 Discussion

During our first day of observing, using only LWA1, we detected 13 unique pulses, while on the last we detected 29 unique pulses using both LWA1 and LWA-SV. We are able to determine which of these pulses are unique because there appears to be a regular 16 or 17 second delay between the pulses in the two frequencies, which is what we would expect to see due to the independent dedispersion of each frequency tuning.

These observations were taken 9 days apart, which allows us to see if there is any change in the τ value over time. We can indeed see a drop of 30 ms or 12.8% when comparing the two LWA1 observations, as well as an increase in the number of pulses detected. This decreasing τ value aligns with the variable nature of the nebula mentioned by Eftekhari et al. 2016. They also saw an increase in the number of detections, which was attributed to the pulse being more concentrated in time, allowing weaker pulses to be more distinguishable from the noise. Seeing both of these trends together is evidence that we are seeing variation in the source rather than a purely

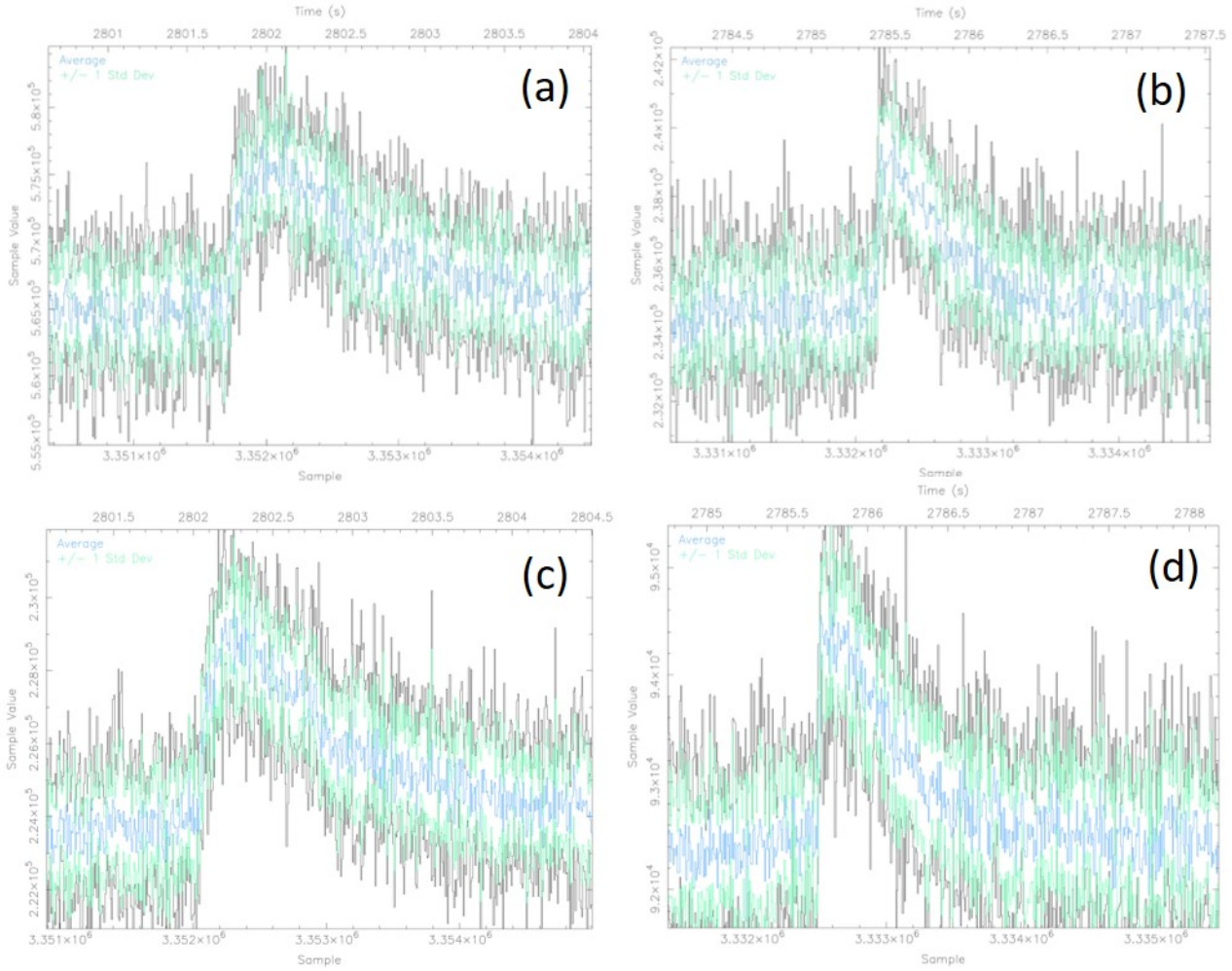

Figure 3: The same pulse profile depicted in four situations: (a) and (b) are from the LWA1 station with 60 and 76 MHz tunings, respectively, and (c) and (d) are from the LWA-SV station with 60 and 76 MHz tunings, respectively.

statistical anomaly.

6.1 Comparison to Prior Results

In the 2016 paper by Eftekhari et al., they observed the same source with the LWA1 for 73 hours, detecting a total of 1,458 pulses or about 20 pulses per hour. This is significantly more than the 10.5 pulses per hour we detected, though this was likely because we searched the data for pulses by eye rather than using a computer algorithm to automatically search for them. Similarly, the τ values they calculated for certain days of observing seemed to decrease over time, shown below in Figure 5.

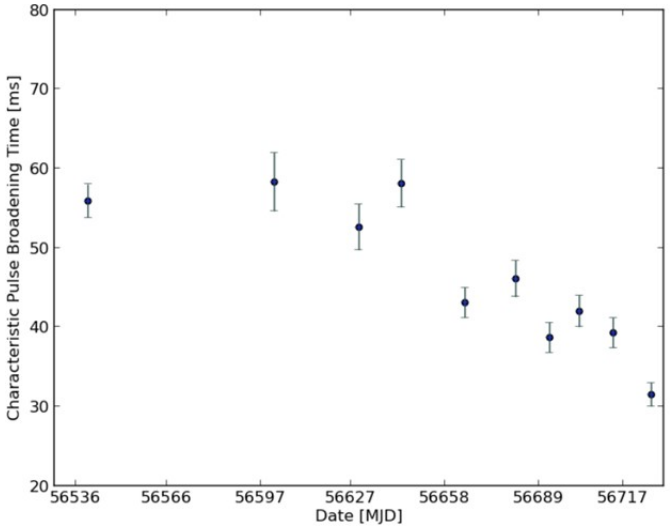

Figure 5: The variation of τ over the span of several months. Credit: Eftekhari et al. (2016)

We saw a similar pattern of the τ value decreasing over time, though we had significantly fewer data points than they did. This again supports the notion that the variability of the nebula would cause the broadening time to vary.

The average τ values that we calculated have been included in Table 3 (in Appendix), where they are compared to past results compiled by Eftekhari et al. (2016). The 60 MHz value of 213 ± 67 ms, and the 76 MHz value of 127 ± 44 ms can be seen to fit in between past observed values, helping to more accurately determine the range where these low frequency values should fall. These previously calculated values varied greatly, so the fact that our values filled in the gap between them helps to show that neither are necessarily outliers.

We can also see these results plotted on Figure 6, where our results fall solidly between results that have previously been recorded with the LWA1. Our results also happen to fall very close to the original line of best fit, as seen on Figure 6. The gray line without our results is defined by $\nu^{-3.45}$, but after including our results, it changes to $\nu^{-3.48}$ (green line). The two data points found in this study help to further constrain the best fit line as well as the dependence of the broadening time on the frequency.

Even though our results don't intersect the error bars of the previous results, this is not particularly concerning, as the varied nature of these values is a large part of why this source is interesting to observe.

6.2 Future Work

Though we observed on 5 separate days, we have only analyzed our observations from the first and last days. Analyzing the rest of these observations is the first step to continue this study, as it will allow us to see if the τ value changed steadily or irregularly. Seeing this value change over a relatively short scale could potentially help us to better understand how it changes, and what that implies about the source of the pulses.

Another avenue for this project in the future could be to observe these giant pulses over a longer timescale. Eftekhari et al. (2016) observed these changes over the course of months, and if we made observations over a similar range of time, it could be used to compare with their longer term results and examine any changes to the number or frequency of the pulses over time.

Another possible application we could attempt to pursue would be to use this data to compare the sensitivities of the LWA1 and LWA-SV

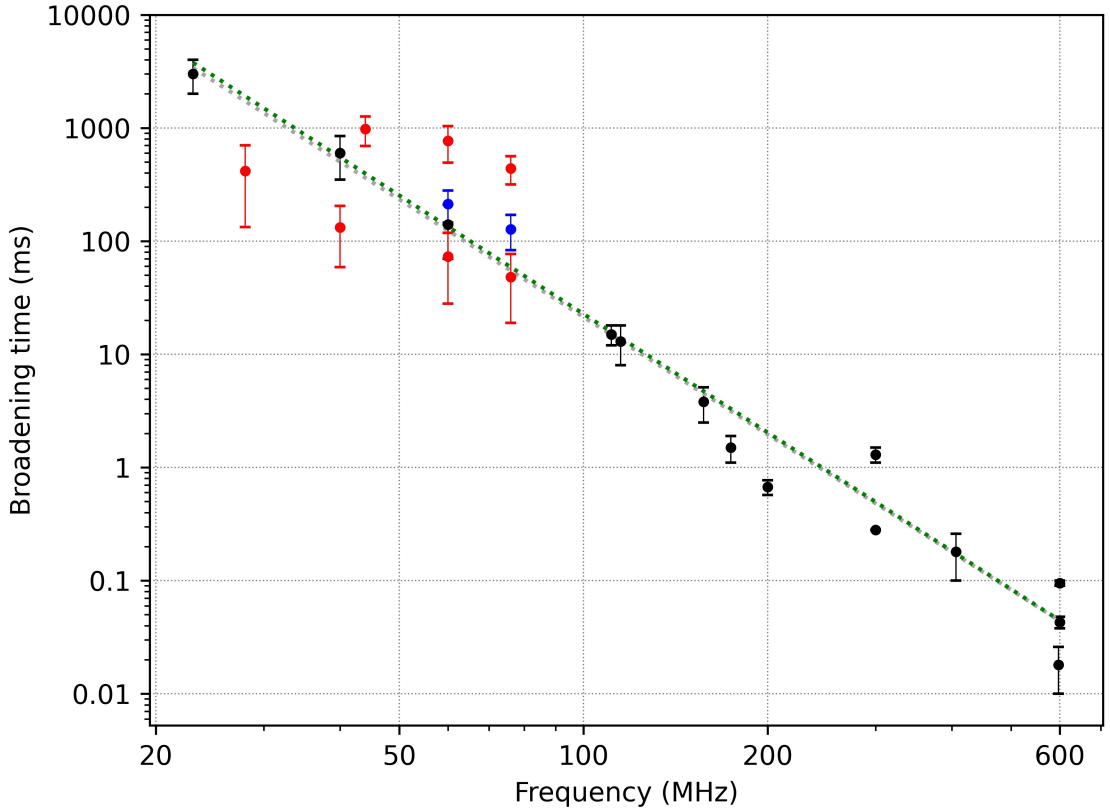

Figure 6: Relationship between τ and frequency. Red points are from previous LWA studies (Eftekhari et al. (2016); Ellingson et al. (2013)), blue points are from this study, and black points are from other low frequency studies. The gray line is the best fit line excluding this work, whereas the green line includes it

stations. By looking at the pulses we detect, we could try to see which station is able to see more pulses, in order to better understand how the two stations compare when observing the same source.

7 Acknowledgements

We would like to acknowledge the help and assistance provided by Dr. Greg Taylor, as well as the insights provided by Pratik Kumar.

References

Bansal, K., Taylor, G. B., Stovall, K., & Dowell, J. 2019, ApJ, 875, 146

Condon, J. J., & Ransom, S. M. 2016, Essential Radio Astronomy (Princeton, NJ: Princeton University Press)

Eftekhari, T., Stovall, K., Dowell, J., Schinzel, F. K., & Taylor, G. B. 2016, ApJ, 829, 62

Ellingson, S. W., Clarke, T. E., Craig, J., et al. 2013, ApJ, 768, 136

Johnston, S., & Romani, R. W. 2004, in Young Neutron Stars and Their Environments, ed. F. Camilo & B. M. Gaensler, Vol. 218, 315

Lorimer, D. R., & Kramer, M. 2004, Handbook of Pulsar Astronomy, Vol. 4 (Cambridge, UK: Cambridge University Press)

Lyne, A. G., Pritchard, R. S., & Graham Smith, F. 1993, MNRAS, 265, 1003

Tan, C. M., Bassa, C. G., Cooper, S., et al. 2018, ApJ, 866, 54

Taylor, J. R. 1997, An Introduction to Error Analysis (Sausalito, CA: University Science Books), 75

A Appendix

Table 1: Pulse statistics for the first day of observation

LWA1 - MJD 059274			
60 MHz		76 MHz	
Time (s)	τ (ms)	Time (s)	τ (ms)
337	277	320	157
702	176	685	105
3975	376	1987	111
4140	177	2715	138
4355	197	3314	125
5157	204	3959	161
5866	273	4123	129
6089	196	4338	140
		4460	163
		5140	102
		5276	146
		5849	175
		6072	200

Table 2: Pulse statistics for the last day of observation

MJD 059282					
	60 MHz			76 MHz	
	LWA-SV	LWA1		LWA-SV	LWA1
Time (s)	τ (ms)	τ (ms)	Time (s)	τ (ms)	τ (ms)
156	214	265	139	53	89
1059	261	274	807	-	166
1442	-	244	1167	194	241
1805	243	178	1352	186	141
2014	126	125	1425	117	168
2080	308	286	1661	-	126
2100	49	122	1683	196	154
2150	-	200	1789	75	80
2567	148	207	2064	157	-
2802	133	178	2084	59	71
3272	249	164	2134	144	154
4036	-	159	2551	120	-
4251	172	209	2785	63	51
5218	356	286	3255	86	112
5539	298	-	4206	191	161
5627	181	124	4235	102	107
6052	218	229	4492	-	131
6771	211	238	5202	124	216
			5244	173	121
			5523	80	89
			5611	117	114
			6036	80	124
			6551	83	126
			6754	37	91

Table 3: τ values for a wide range of frequencies

ν (MHz)	τ (ms)	Reference
23	3000 ± 1000	Popov et al. (2006)
28	417 ± 284	Eftekhari et al. (2016)
40	132 ± 73	Eftekhari et al. (2016)
40	600 ± 250	Kuzmin et al. (2002)
44	978 ± 287	Ellingson et al. (2013)
60	140 ± 70	Kuzmin et al. (2002)
60	768 ± 273	Ellingson et al. (2013)
60	73 ± 45	Eftekhari et al. (2016)
60	213 ± 67	*This work*
76	127 ± 44	*This work*
76	439 ± 122	Ellingson et al. (2013)
76	48 ± 29	Eftekhari et al. (2016)
111	15 ± 3	Popov et al. (2006)
115	13 ± 5	Staelin & Sutton (1970)
157	3.8 ± 1.3	Staelin & Sutton (1970)
174	1.5 ± 0.4	Karuppusamy et al. (2012)
200	0.670 ± 0.100	Bhat et al. (2007)
300	1.3 ± 0.2	Sallmen et al. (1999)
300	0.28	Sallmen et al. (1999)
406	0.18 ± 0.08	Kuzmin et al. (2002)
594	0.018 ± 0.008	Kuzmin et al. (2002)
600	0.095 ± 0.005	Sallmen et al. (1999)
600	0.043 ± 0.005	Popov et al. (2006)